The effect of fin spacing and material on the performance of a heat sink with circular pin fins

A Dewan*, **P Patro, I Khan,** and **P Mahanta**
Department of Mechanical Engineering, Indian Institute of Technology Guwahati, Guwahati, Assam, India

The manuscript was received on 17 January 2009 and was accepted after revision for publication on 15 July 2009.

DOI: 10.1243/09576509JPE750

Abstract: This article presents a computational study of the steady-state thermal and air-flow resistance characteristics and performance analysis through a rectangular channel with circular pin fins attached to a flat surface. The pin fins are arranged in staggered manner and the heat transfer is assumed to be conjugated in nature. The body forces and radiation effects are assumed to be negligible. The hydrodynamic and thermal behaviours are studied in detail for the Reynolds numbers varying from 200 to 1000. The heat transfer increases with an increase of the fin density along the streamwise direction. For the same surface area and pumping power, the fin materials with large thermal conductivity provide high heat transfer rate with no increase in the pressure drop. The emphasis of the present research work is not only to look into the traditional objective of maximum heat transfer in a heat exchanger, but also to obtain it with minimum pressure drop.

Keywords: heat exchanger, computational fluid dynamics, turbulent flow, wall function, pressure drop

1 INTRODUCTION

Heat exchangers are the equipment used to transfer thermal energy from a hot fluid to a cold fluid, in most cases through an intermediate metallic wall. Heat exchangers are basically heat convection equipment, because it is the convective transfer that governs their performance. Convection within a heat exchanger is always forced and may be with or without phase change of one or both fluids. Compact heat exchangers (CHEs) offer a high surface area-to-volume ratio typically more than $700\,m^2/m^3$ for gas–gas applications and more than $400\,m^2/m^3$ for liquid–gas applications. This means that a CHE must contain a number of extended surfaces. Pin fins are commonly used as extended surfaces in CHEs to augment heat transfer and turbulence. CHEs are used in a wide variety of applications including air-conditioning condensers and evaporators and automotive radiators and many others. The pin-fin heat exchanger considered in the present article is the one that is widely used for the cooling of electronic appliances. During the past two decades, rapid advances in micro fabrication techniques have taken place. Some manufacturing techniques that are used for the fabrication of electronic circuits are being used for the fabrication of compact heat exchangers. An understanding of the effect of the fluid velocity on the performance of the heat exchanger is of paramount importance for the design and characterization of electronic systems.

Extensive research on pin-fin CHEs has been going on for more than five decades. Kays [**1**] performed an extensive study of compact heat exchanger and derived several correlations for the heat exchanger's thermal performance and flow behaviour. Dewan *et al.* [**2**] have presented a review of different methods that can be adopted for the enhancement of heat transfer in heat exchangers. Maudgal and Sunderland [**3**] performed an experimental investigation of forced convection heat transfer for inline pin-fin arrays. A comparison of performance of different pin-fin geometries in laminar forced convection was performed by Behnia *et al.* [**4**]. The performance of an array of staggered and inline cooling fins was compared by Leon *et al.* [**5**]. The results showed the advantages of the staggered model compared with the inline model, because for a given incoming velocity, the use of a staggered heat sink always leads to a maximization of the heat transfer flux. Short *et al.* [**6**]

* *Corresponding author: Department of Applied Mechanics, Indian Institute of Technology Delhi, Hauz Khas, New Delhi 110016, India. email: adewan@iitg.ernet.in; adewan@daad-alumni.de*

showed that at low to moderate Reynolds numbers, cast pin-fin cold walls provide the best performance and also involve a low cost for electronic applications. A comprehensive theoretical and experimental study was carried out on the thermal performance of a pin-fin heat sink by Kobus and Oshio [**7**]. They formulated a theoretical model that has the capability of predicting the influence of various geometrical, thermal, and flow parameters on the effective thermal resistance of the heat sink. The steady-state thermal and air-flow resistance performances of horizontally based pin-fin assemblies were investigated experimentally by Tahat *et al.* [**8**]. They studied the effects of varying the geometrical configurations of the pin-fin and the air-flow rates. Sahiti *et al.* [**9**] reviewed some important methods proposed in the literature for comparison of different elements for heat-transfer enhancement. Sahiti *et al.* [**10**] demonstrated that the use of cylindrical pin fins in heat exchangers amounts to considerable enhancement in heat transfer. Some of the other researchers who investigated the cylindrical pin fins include Sparrow *et al.* [**11**], Metzer *et al.* [**12**], and Moshfegh and Nyiredy [**13**].

Dewan *et al.* [**14**] compared their numerical results using three turbulence models, namely, the standard k–ε model, the renormalization group (RNG) k–ε model, and the realizable k–ε model, with the experimental data reported in the literature and a good agreement was obtained using RNG k–ε model with the standard wall functions. Experimental investigation of the fluid dynamics of the pin-fin arrays in order to clarify the physics of heat transfer enhancement was performed by Ames and Dvorak [**15**]. They observed that in early rows where turbulence is low, the strength of shedding increases dramatically with Reynolds number. The laminar velocity profiles off the surface of pins show evidence of unsteady separation in early rows. In the third row and beyond, laminar boundary layers off pins are quite similar.

Advantages of the staggered array over inline array were shown by Dvinsky *et al.* [**16**]. An experimental, numerical, and analytical study of the optimal spacing between cylinders in cross-flow forced convection was carried out by Stanescu *et al.* [**17**]. The optimal cylinder-to-cylinder spacing was determined by maximizing the overall thermal conductance between all the cylinders and the free stream. According to Zukauskas and Ulinskas [**18**], at low $Re < 10^3$, the mainstream flow within the bank of tubes is laminar with regions of circulating macroscale eddies whose effect on the boundary layer over the front part of tubes is attained by viscous forces and the favourable pressure gradient. This flow pattern over a tube bank that occurs at $Re < 10^3$ can be regarded as predominantly laminar with large-scale vortices in the recirculation regions. With a further increase in Re, intertube flow becomes highly turbulent with intensity depending on the bank configuration. For long tube arrays, Zukauskas [**19**] reported that reducing the streamwise spacing increases heat transfer, and though less significantly, increasing the spanwise spacing increases the heat transfer.

Larson and Sparrow [**20**] compared the performance among geometrically different pin-fin arrays situated in an oncoming longitudinal flow. An experimental investigation was conducted by Ames *et al.* [**21**] in a staggered-pin-fin array at Reynolds numbers of 3000, 10 000, and 30 000 based on the maximum velocity between cylinders. Turbulence measurements and velocity distributions were acquired at the inlet and in between adjacent pins in rows using hot wire anemometry. Lu and Jiang [**22**] experimentally and numerically investigated the heat transfer in a rectangular channel with angled ribs. The ribs were taken at various angles and the comparison between the experimental and numerical results showed that the shear stress transport (SST) k–ω turbulence model was suitable for the convection heat transfer in such channels.

It has been observed experimentally by Incropera [**23**] that the flow around a cylinder can be approximated as the flow around a single pin in cross flow. Tahat *et al.* [**24**] investigated experimentally the steady-state thermal and hydraulic performances of horizontally based pin-fin assemblies. They studied the effects of varying the geometrical configurations of the pin-fins and the air-flow rates. Mon and Gross [**25**] numerically studied the fin-spacing effects in annular-finned tube heat exchangers. The study by Yang *et al.* [**26**] examined the thermal–hydraulic performance of heat sinks. They performed a comparison of the associated heat-transfer performance and the effect of fin spacing. Sahin [**27**] investigated the effect of inlet air velocity, thermal properties of the working fluid and the pin fins, the relative pin-fin height, the cross-sectional shape of the pin fins by using the Taguchi approach for a circular pin-fin heat exchanger. Babus'Haq *et al.* [**28**] experimentally investigated steady-state forced-convective cooling of a horizontally based pin-fin assembly. Goldstein *et al.* [**29**] have provided an excellent review of heat transfer enhancement, including numerical, analytical, and experimental studies.

The literature survey shows that the effects of pin-fin geometry, inlet air velocity, and different turbulence models on the performance of a heat exchanger have been investigated by many researchers. In the present article, the effects of streamwise fin spacing and pin-fin material on the thermal and fluid performances of the heat exchanger are investigated numerically. The computations were performed using the commercial computational fluid dynamics (CFD) package FLUENT 6.3. The effect of the streamwise fin spacing S is carried out for $S/d = 2.3$, 3.13, and 4.0 (where S denotes the longitudinal fin spacing and d the fin diameter) and $H/d = 10$ (where H denotes the fin height). Three fin materials, namely, aluminium,

nickel, and steel, are used for studying the effect of fin material thermal conductivity.

2 COMPUTATIONAL DOMAIN AND GOVERNING EQUATIONS

The computational domain considered in the present study is a three-dimensional rectangular duct with a staggered array of circular pin fins mounted on the heated bottom wall maintained at a constant temperature. A schematic of the pin-fin heat sink model used in the present study is shown in Fig. 1.

To simplify the analysis, two adjacent rows of fins were considered. Two planes along the middle of these two rows of fins were passed and the flow and thermal behaviours were assumed to be symmetric across these planes (Fig. 2). With laminar flow through the heat exchanger, this symmetry boundary condition would perhaps be more reasonable than that for the case of turbulent flow. Under turbulent flow conditions, possible vortex shedding in the wake of pins may give rise to flow asymmetry and therefore some inaccuracies may be introduced if the symmetry conditions are applied. Nevertheless, the symmetry boundary conditions were applied to save the computational effort (for example, see references [**4**], [**14**], [**15**], and [**30**]).

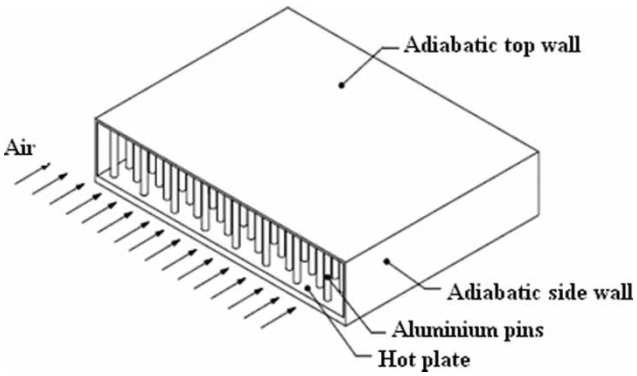


Fig. 1 Pin-fin heat sink model

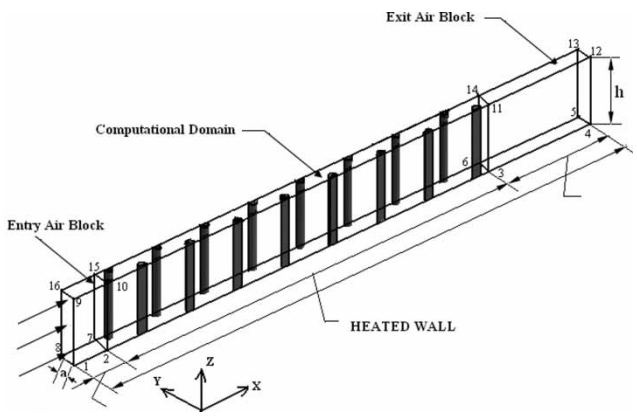


Fig. 2 Computational domain considered in the present article

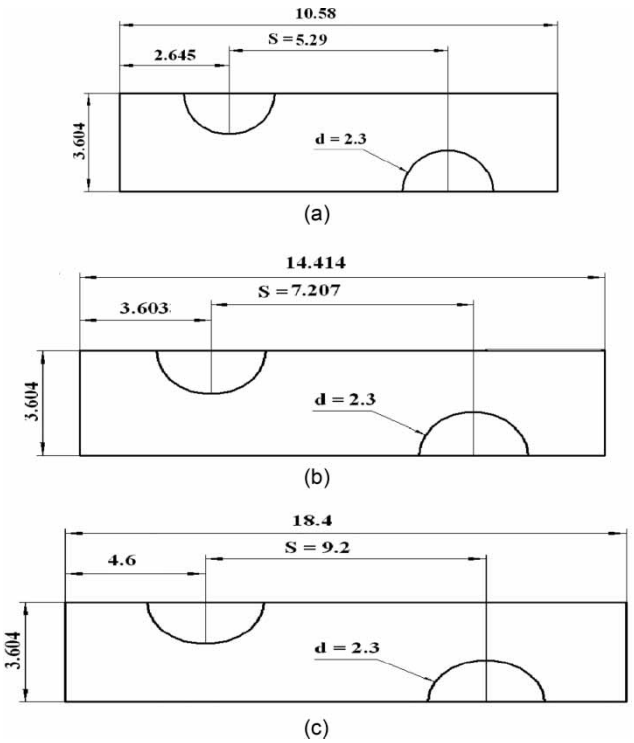


Fig. 3 Dimensions of unit cells for three configurations (all dimensions are in mm)

The computational domain as shown in Fig. 2 has a width $a = 3.6$ mm, flow length $L = 155.3$ mm, and fin height $H = 23.0$ mm. The fins have the circular cross-sections. The diameter of the fins d is 2.3 mm. A hydraulic diameter D_h of 2.0 mm was used as this value is commonly used for the pin fins used in electronic appliances. The length of the flow developing inlet block was taken to be $5D_h$, whereas the outlet block length was set equal to $15D_h$ in order to avoid any influence of the eventual back flow streams on behaviour in the heat exchanger [**30**, **31**].

To study the effect of streamwise fin spacing, three configurations were selected. The corresponding unit cells are shown in Fig. 3. Table 1 provides number of fins considered in three configurations. The volume of the computational domain considered was the same for the three configurations.

2.1 Governing equations

For an incompressible steady flow and neglecting body forces, the governing mass continuity and momentum

Table 1 S/d ratio and number of fins considered in three cases in the present study

Configuration	S/d	Number of fins
A	2.30	22
B	3.13	16
C	4.00	13

equations can be written in the Cartesian tensor form as

$$\frac{\partial(\rho u_i)}{\partial x_i} = 0 \tag{1}$$

$$\rho u_j \frac{\partial u_i}{\partial x_j} = -\frac{\partial p}{\partial x_i} - \frac{\partial(-\overline{u_j' u_i'})}{\partial x_j} \tag{2}$$

The Reynolds stress tensor is given by

$$-\overline{u_j' u_i'} = 2\mu_t \left(\frac{\partial u_i}{\partial x_j} + \frac{\partial u_j}{\partial x_i}\right) - \frac{2}{3}\rho\delta_{ij}k \tag{3}$$

here μ_t denotes the eddy viscosity and $i, j = 1, 2,$ and 3.

The governing equation for obtaining the temperature field is provided by

$$\rho c_p u_i \frac{\partial T}{\partial x_i} = k_f \frac{\partial^2 T}{\partial x_i^2} - \frac{\partial}{\partial x_i}(\rho c_p \overline{u_i' T'}) \tag{4}$$

where u_i denotes the velocity components in the Cartesian coordinate system with its coordinates x_i, T_f the fluid temperature, p the pressure, and k_f the thermal conductivity of the fluid.

The conjugate heat transfer from pin-fin arrays was assumed in all cases considered in the present article. It implies the simultaneous solution of equations (1) to (4) and the energy equation in the solid, which reads

$$\frac{\partial^2 T_s}{\partial x_i^2} = 0 \tag{5}$$

The RNG k–ε model was used to model turbulence [**14**]. The transport equations for turbulence kinetic energy k and its rate of dissipation ε used in the RNG k–ε model are

$$\frac{\partial}{\partial t}(\rho k) + \frac{\partial}{\partial x_i}(\rho k u_i) = \frac{\partial}{\partial x_j}\left(\frac{\mu_{eff}}{\sigma_k}\frac{\partial k}{\partial x_j}\right) + G_k - \rho\varepsilon \tag{6}$$

$$\frac{\partial}{\partial t}(\rho\varepsilon) + \frac{\partial}{\partial x_i}(\rho\varepsilon u_i) = \frac{\partial}{\partial x_j}\left(\frac{\mu_{eff}}{\sigma_\varepsilon}\frac{\partial \varepsilon}{\partial x_j}\right) + C_{1\varepsilon}\frac{\varepsilon}{k}G_k - C_{2\varepsilon}\rho\frac{\varepsilon^2}{k} - R_\varepsilon \tag{7}$$

$$R_\varepsilon = \frac{c_\mu \rho \eta^3 (1 - \eta/\eta_0)}{1 + \beta\eta^3}\frac{\varepsilon^2}{k}\quad \eta = S\frac{k}{\varepsilon} \tag{8}$$

The model constants are $C_\mu = 0.0845$, $C_{1\varepsilon} = 1.42$, $C_{2\varepsilon} = 1.68$, $\sigma_k = \sigma_\varepsilon = 0.7178$, and $\beta = 0.012$.

Turbulent heat fluxes in the thermal energy equation are modelled as

$$-\rho\overline{u_i' T'} = -\frac{\mu_t}{Pr_t}\frac{\partial T}{\mathrm{d}x_i} \tag{9}$$

The eddy viscosity in equations (3) and (9) is computed as

$$\mu_t = \rho C\mu k^2/\varepsilon \tag{10}$$

The standard law of the wall was used to model the turbulence close to the wall. The law of the wall for temperature used in the present work is of the following form

$$T^+ = Pr[\ln(EY^+) + P] \tag{11}$$

$$P = 9.24\left[\left(\frac{Pr}{Pr_t}\right)^{3/2} - 1\right](1 + 0.28e^{-0.007Pr/Pr_t}) \tag{12}$$

Here Pr_t is the turbulent Prandtl number and is taken as 0.85 and $Pr = 0.71$ for air. The physical properties of air considered are $\rho = 1.225\,\mathrm{kg/m^3}$, $\mu = 1.789 \times 10^{-5}\,\mathrm{kg/(m\,s)}$, and $C_p = 1006.43\,\mathrm{J/kg/K}$ [**32**].

2.2 Boundary conditions

The inlet (velocity inlet), outlet (pressure outlet), wall and symmetry boundary conditions were applied in the computational domain. The boundary conditions referring to Fig. 2 are:

(a) For the inlet section 1–8–16–9

$$u(0, y, z) = u_{in},\ v(0, y, z) = 0, w(0, y, z) = 0$$

and

$$T(0, y, z) = T_{in} = 293\,\mathrm{K} \tag{13}$$

(b) For the bottom heated wall 2–3–6–7

$$u(x, y, 0) = v(x, y, 0) = w(x, y, 0) = 0 \quad \text{and}$$
$$T(x, y, 0) = T_w = 343\,\mathrm{K} \tag{14}$$

(c) For the section 1–4–5–8

$$u(x, y, 0) = v(x, y, 0) = w(x, y, 0) = 0 \quad \text{and}$$
$$\left(\frac{\partial T}{\partial z}\right)_{x,y,0} = 0 \tag{15}$$

(d) The top wall 9–12–13–16 was considered to be adiabatic, where the no slip condition for the velocity components was applied

$$u(x, y, z) = v(x, y, z) = w(x, y, z) = 0 \quad \text{and}$$
$$\left(\frac{\partial T}{\partial z}\right) = 0 \tag{16}$$

(e) For sections 1–4–12–9 and 8–5–13–16, the symmetry boundary condition [**4**, **14**, **15**, **30**] was applied and in the outlet section 4–12–13–5 the pressure outlet boundary condition was used.

3 NUMERICAL SIMULATION

The governing equations along with the boundary conditions were solved numerically by the finite volume method using a commercial CFD software FLUENT 6.3. The second-order upwind scheme was used to discretize the governing equations. The preprocessing tool Gambit was used for the creation of geometry

and meshing. Based on the study by Dewan *et al.* [**14**] the RNG k–ε model with the standard wall functions was used in the present study. The segregated solver was employed to obtain the numerical solution of the governing equations for the conservation of the mass, momentum, and energy and other scalar variables, such as turbulence. The SIMPLE algorithm was used to relate velocity and pressure corrections to enforce mass conservation and to obtain the pressure field. Sutherland's correlation was used for the molecular viscosity of air [**30**, **32**]

$$\mu = \left(\frac{T}{273.15}\right)^{3/2} \frac{273.15 + C_s}{T + C_s} \mu_0 \tag{17}$$

where μ_0 denotes the dynamic viscosity at 273.15 K and 1.013 25 bar, C_s is the Sutherland constant, and T the absolute temperature. The properties of the solid fins were considered to be constant.

3.1 Mesh and grid independence

A mesh of size 810 000 was used to carry out the computations. This size was based on the grid independence study performed by Dewan *et al.* [**14**]. A tetrahedral mesh was obtained from the triangular meshes on the surfaces. Turbulence plays a dominant role in the transport of mean momentum and other properties. Therefore turbulent quantities in complex turbulent flows should be properly resolved, and in the present work we have resolved, with sufficiently fine meshes, the regions where the mean flow changes rapidly and there are shear layers with a large mean rate of strain. We can assess the near-wall mesh from the values of non-dimensional distance from the wall $y^+ = \rho u_\tau y/\mu$. For the standard wall function, each wall adjacent cell's centroid should be located within the log-law layer, $30 < y^+ < 300$. However, a value of y^+ close to 30 is desirable. A variation of y^+ for the wall adjacent cell's centroid along the computational domain for the present computation shows that y^+ varies from 35 to 41, which means that the first grid point is located in the log layer (Fig. 4).

3.2 Validation

The validation of the code in the present study was performed by comparing the computations with the experimental data of Kays [**1**] for the Nusselt number and Colburn factor (Fig. 5). The present predictions by

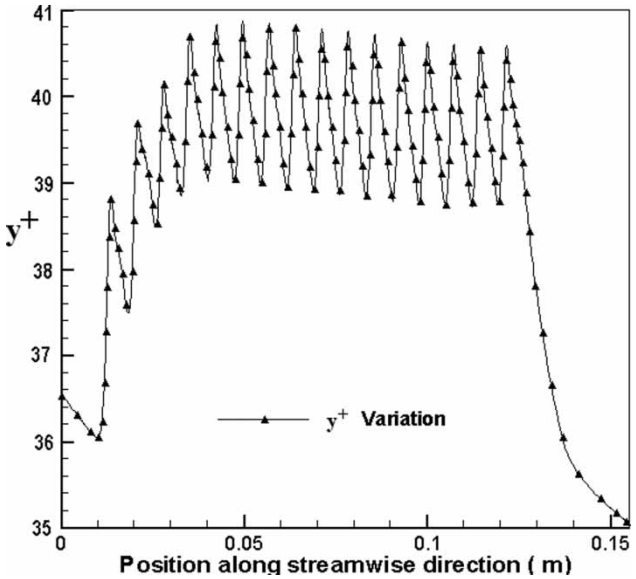


Fig. 4 Non-dimensional distance from the wall along the computational domain for the present computation

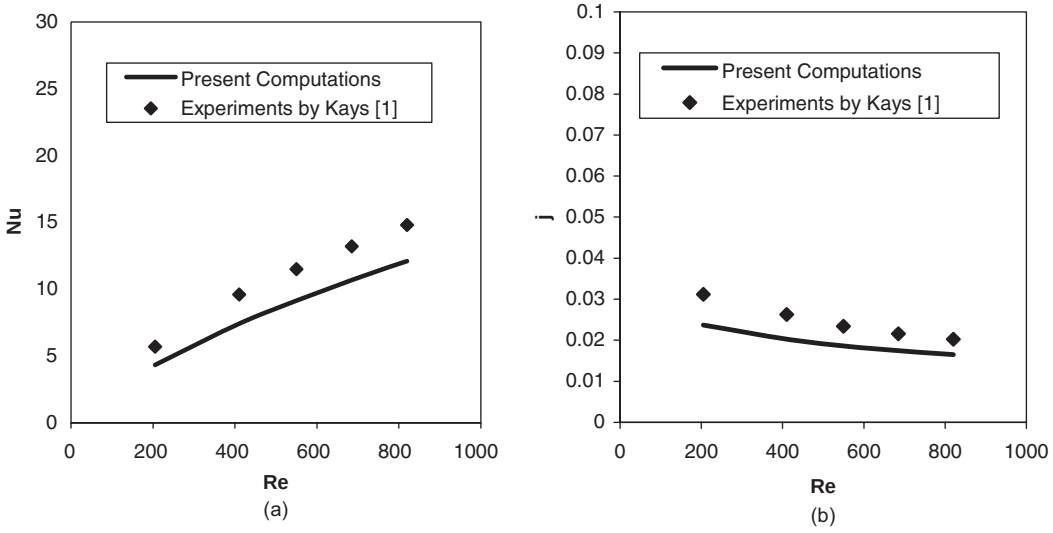


Fig. 5 Validation of the present computations with experimental data by Kays [**1**]: (a) Nusselt number and (b) Colburn factor

the RNG k–ε model using the standard wall function are in reasonably good agreement with the experimental data [**1**]. An average deviation of approximately 20 per cent between the two can be attributed to experimental uncertainties and limitation of modelling complex turbulent flow in this heat exchanger using the Reynolds-averaged Navier–Stokes (RANS) equations. The amount of deviation obtained in the present article is similar to that obtained in the literature for the validation of computational model for circular pin-fin heat sink [**30**, **31**].

4 RESULTS AND DISCUSSION

4.1 Flow behaviour in a pin-fin heat exchanger

Incropera [**23**] observed experimentally that the flow around a cylinder can be approximated as the flow around a single pin in a cross flow. Therefore the flow over an assembly of circular pin fins is approximated as a flow over a bank of tubes. The flow over a bank of tubes is more complex than that over a single tube, due to non-uniformity of the velocity field, high turbulence, and other factors including longitudinal and transverse pitches. Flow over tubes within a bank involves significant blockage of the flow passage. When a bank of tubes is placed in a real fluid, a laminar boundary layer develops on the leading surfaces due to viscous forces. As the Reynolds number is increased the flow separation occurs and recirculation takes place towards the trailing edge.

The flow behaviours of the pin fins in the present study for different Reynolds numbers are shown in the form of vorticity contours in Fig. 6. The fin considered here is the one in the third row of the computational domain. The flow considered here is laminar and no turbulence model was used to obtain these velocity vectors. It is observed that for $Re \leqslant 15$ the cylinder is enveloped by a laminar boundary layer, which separates only at the rear stagnation point. An increase in Re causes the separation to occur at a certain distance from the rear stagnation point due to increase in the inertial forces.

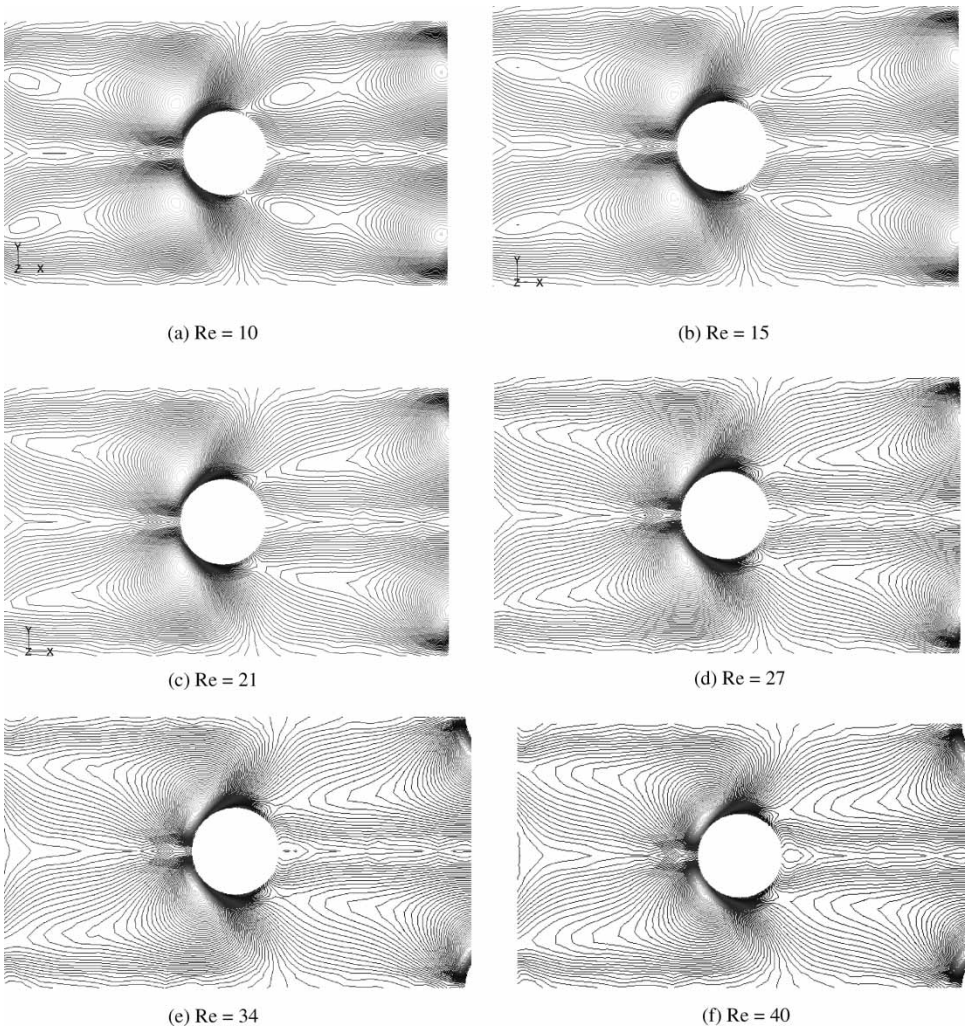


Fig. 6 Vorticity contours at different Reynolds numbers

The flow behaviour changes at Reynolds number 20–25. Flow separation occurs and recirculation of fluid takes place towards the trailing edge of the fins. The turbulent eddies are formed and the intensity of the turbulent eddies and recirculation is significant when *Re* is higher than 40. The wake behind the cylinder becomes unstable and vortex shedding is initiated. As *Re* increases further, the point of separation gradually moves upstream. Therefore the Reynolds number should be more than 40 for proper mixing of the fluid to augment the heat transfer in a heat exchanger. For the present computation, Reynolds number was varied from 200 to 1000.

4.2 Effect of fin material

Three fin materials namely, aluminium, nickel and steel were considered to study the effect of pin fin's thermal conductivity on the performance of the heat exchanger. As already stated in Section 3.1 conjugate heat transfer from pin-fin arrays was assumed while considering the effect of the fin material. The characteristics of the convective heat transfer from pin arrays can be understood from the temperature contours in fluid and solid parts of the computational domain (Fig. 7). It is seen that the fluid adjacent to the fins attain the maximum temperature. Heat is transferred from the bottom heated plate to the fins by conduction and from fins to the fluid by turbulent convection. The temperature difference between the fin and the fluid decreases in the downstream direction. The fluid takes heat from the fins and hence the temperature of the fluid increases. It was observed that for the aluminium fins, the exit temperature of the fluid is the maximum and for steel fins it is the minimum. The temperature difference between the fins and the surrounding fluid decreases along the computational domain. The global Nusselt number is more for aluminium fins compared to that for the other two fins (Tables 2 to 4). It was also observed that as the inlet velocity increases, the outlet bulk temperature decreases for all cases due to large convective heat transfer at high inlet velocity.

Table 2 Heat transfer and pressure drop for aluminium fins

Reynolds number, *Re*	205.0	410.0	550.0	685.0	820.0
Present Nusselt number, *Nu*	4.34	7.42	9.14	10.69	12.1
Nusselt number, *Nu*, from experimental data by Kays [**1**]	5.7	9.6	11.5	13.2	14.8
Total pressure drop, Δp (Pa)	19.93	66.69	109.88	162.52	224.20

Table 3 Heat transfer and pressure drop for nickel fins

Reynolds number, *Re*	205.0	410.0	550.0	685.0	820.0
Present Nusselt number, *Nu*	3.81	6.20	7.53	9.61	10.12
Total pressure drop, Δp (Pa)	19.89	66.56	109.66	162.25	223.88

Table 4 Heat transfer and pressure drop for steel fins

Reynolds number, *Re*	205.0	410.0	550.0	685.0	820.0
Present Nusselt number, *Nu*	2.612	3.82	4.61	5.18	5.41
Total pressure drop, Δp (Pa)	19.75	65.10	108.81	161.05	222.36

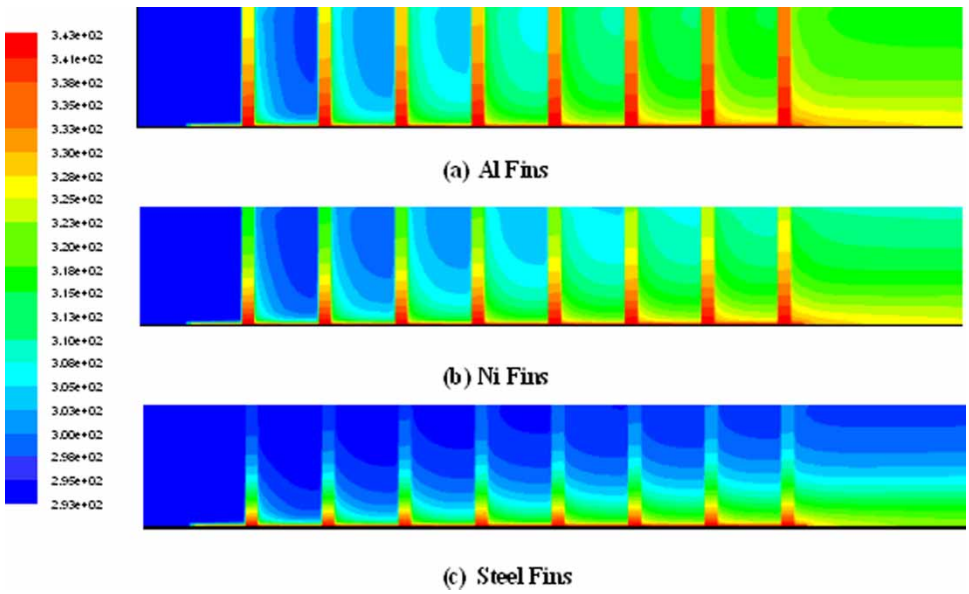


Fig. 7 Temperature contours on the x–z plane ($y = 0$) for the inlet velocity of 3.0 m/s

Overall Nusselt numbers and total pressure drop at different Reynolds numbers for three fin materials are presented in Tables 2–4. The total pressure drop is directly related to the input power required to drive the fan of a compact heat exchanger. The Nusselt number obtained experimentally by Kays [**1**] for aluminium fins is also shown in Table 2. To the best of the authors' knowledge no experimental data for nickel and steel fins exist in the literature and therefore no comparison can be made. Table 2 shows that the present predictions of the aluminium fins are in reasonably good agreement with the experimental data of Kay [**1**]. Possible reasons for the deviation between the present predictions and experimental data have already been given in Section 3.2.

Tables 2 to 4 show that the Nusselt number increases with Reynolds number and simultaneously pressure drop also increases. Up to $Re = 685$, which corresponds to an inlet velocity of 5.0 m/s, the pressure drop rises slowly. However, for higher values of Re the rise in pressure drop is high compared with a corresponding small rise in Nusselt number in all the three cases. Therefore a compact heat exchanger should be operated at approximately 4.0–5.0 m/s inlet velocity. The total heat transfer is the highest for the aluminium fins and the lowest for the steel fins at different Reynolds numbers. The pressure drop is approximately the same for all the three cases indicating that there is hardly any change in the hydrodynamic behaviour with a change in thermal conductivity. An extremely small change in the pressure drop is probably due to a small change in the hydrodynamic behaviour due to a change in the viscosity of air due to temperature.

4.3 Effect of streamwise fin spacing

The three geometries chosen for this purpose are shown in Fig. 3 and the corresponding values of S/d and number of fins considered are shown in Table 1. The computations were carried out for the Reynolds numbers from 200 to 1000.

The corresponding temperature contours are shown in Fig. 8. It has been seen that for streamwise spacing $S/d = 2.3$, the heat transfer from the fins to the bulk of the fluid is more compared with that for the other two cases. This is due to large heat transfer area available in this case for the same volume of the heat exchanger. As the flow velocity increases, the bulk temperature of the fluid decreases.

Upstream of the pin fins, there is ordinary duct flow, which may be laminar or turbulent depending on the duct Reynolds number. With a turbulent flow approaching the pin-fin row, the flow is accelerated between the pin fins. This increases the velocity between the pins (this is clearly observed from Fig. 9) and it increases the transfer of energy between the pin-fin row and the fluid. Turbulent wakes are shed from the pin fins and enhance the duct wall heat transfer downstream of the pin-fin row. The heat transfer is higher within the pin wakes as opposed to that between the pins. Downstream the individual wakes from the pins tend to disperse and the flow begins to redevelop and become uniform in the transverse direction to the bulk flow. Heat transfer and pressure drop characteristics for the three configurations are shown in Figs 10 and 11. As the number of fins in the computational domain is increased (i.e. by decreasing

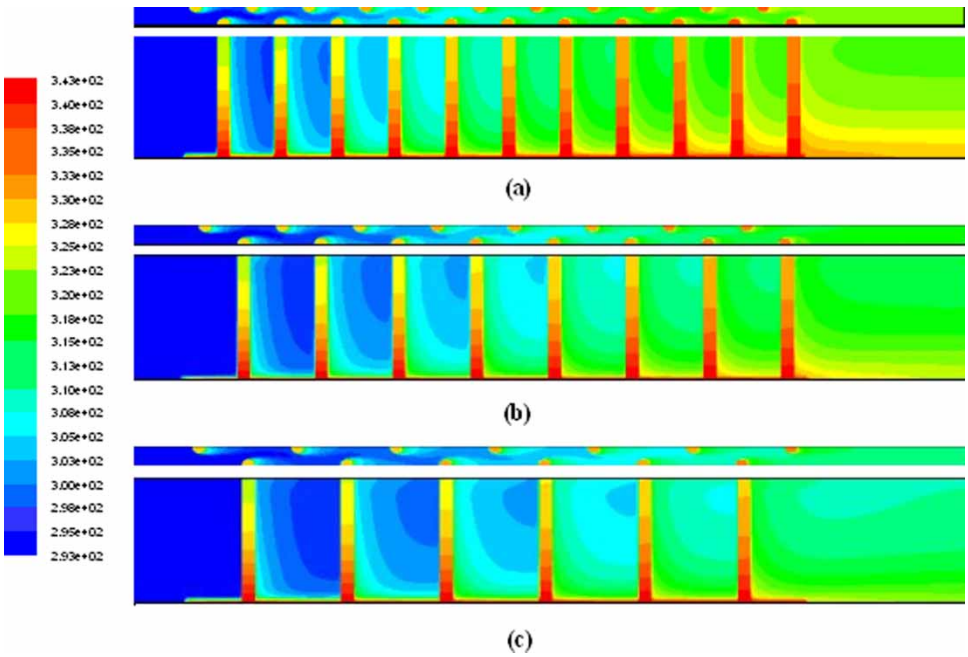


Fig. 8 Temperature contours: (a) $S/d = 2.3$; (b) $S/d = 3.13$; and (c) $S/d = 4.0$ at 4.0 m/s ($Re = 550$)

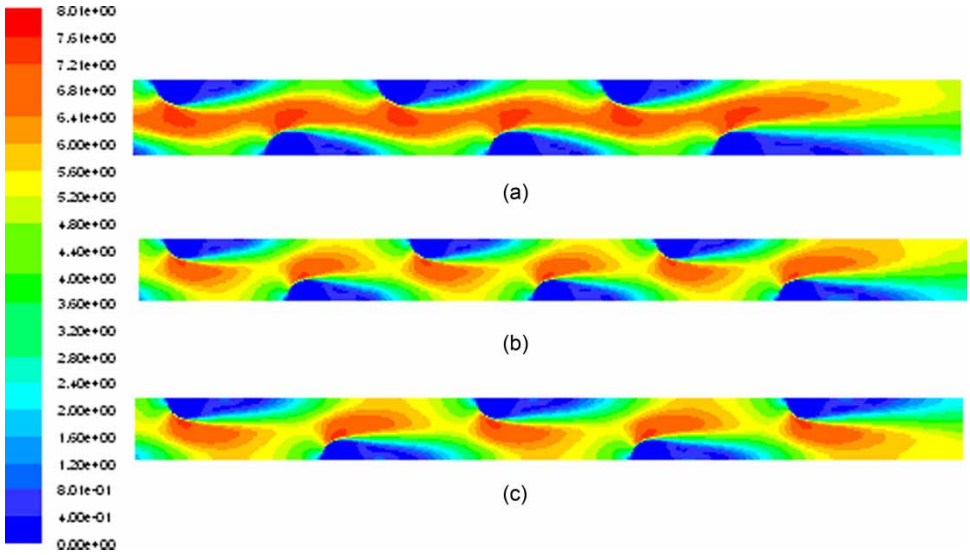


Fig. 9 Velocity contours at 4.0 m/s ($Re = 550$): (a) $S/d = 2.3$; (b) $S/d = 3.13$; and (c) $S/d = 4.0$

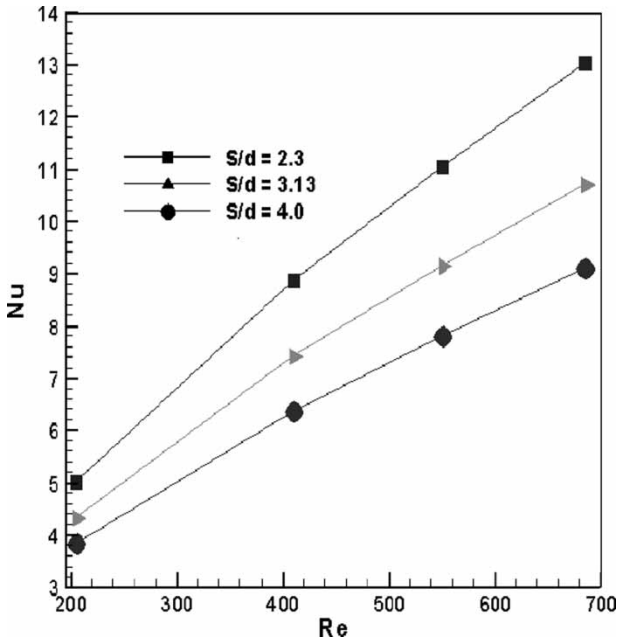


Fig. 10 Variation of global Nusselt numbers with Reynolds numbers

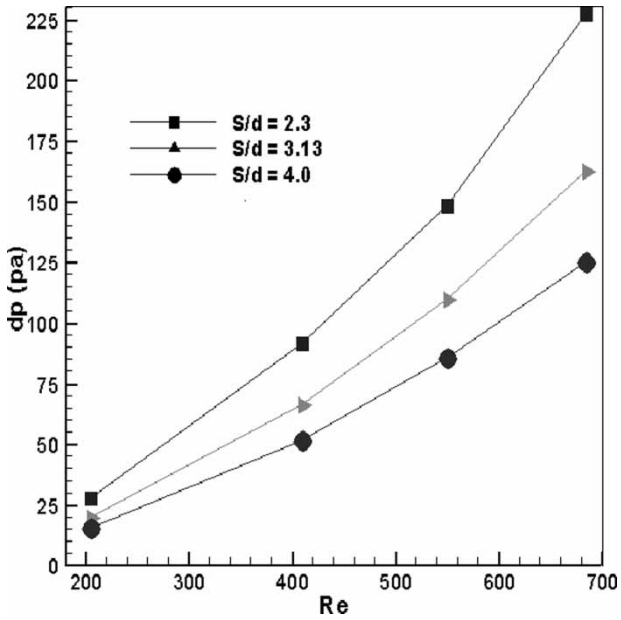


Fig. 11 Variation of pressure drop with Reynolds numbers

the row-to-row spacing) the heat transfer increases and this is accompanied by a corresponding rise in the pressure drop. The air flow around a pin-fin array encounters a significant resistance and hence an overall pressure drop. A larger rate of heat transfer is achieved by increasing the inlet velocity. At high *Re*, the difference of heat transfer at different fin spacings is large (Fig. 10).

Figure 12 shows the static temperature variation for the three fin spacings. For all the three cases the temperature increases towards the exit. The exit temperature is largest for $S/d = 2.3$ and therefore large heat transfer takes place. Static pressure behaves just opposite to the temperature and it decreases along the computational domain. We observe from Fig. 13 that the pressure drop is also large for $S/d = 2.3$. Colburn factor j represents non-dimensional form of heat transfer and it is a standard practice in the literature to present this parameter as a function of Reynolds number [**33**]. Figure 14 shows that the Colburn factor j is the largest for the smallest fin spacing for the entire range of Reynolds number and this is consistent with the static temperature data presented in Fig. 12.

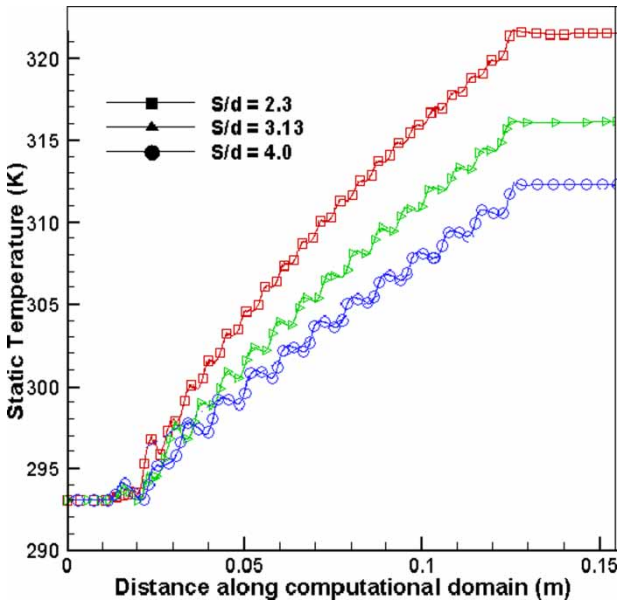


Fig. 12 Static temperature variation

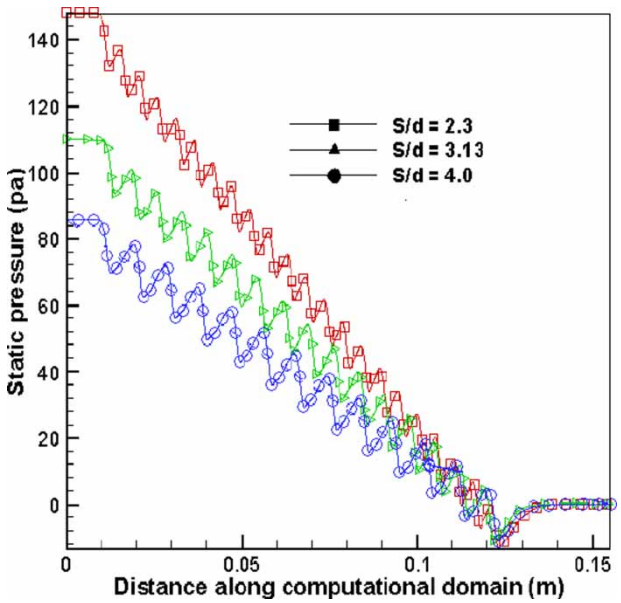


Fig. 13 Static pressure variation

5 CONCLUSIONS

A computational study to understand the thermo-fluid behaviour of a circular heat exchanger has been presented using the RNG k–ε turbulence model and standard wall functions. The conclusions may be summarized as follows:

1. Considering different factors for a compact heat exchanger, such as heat transfer, pressure drop, density, etc., aluminium is found to be the best fin material.
2. Reynolds numbers from 550 to 685 are the best for operating a compact heat exchanger. Although heat transfer increases by increasing *Re* to more than 685, the proportion by which the corresponding heat transfer increases is small compared with the proportion by which total pressure drop increases.
3. As far as the magnitude of heat transfer is concerned, the fin spacing with $S/d = 2.3$ provides much higher augmentation than that for $S/d = 3.13$ and 4.0. The results show that the heat transfer decreases with an increased fin spacing. These differences are caused by decreased fin wake interactions with increased fin spacings.

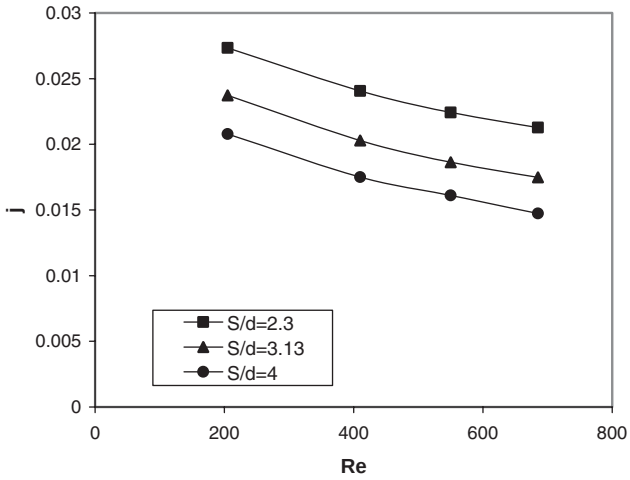


Fig. 14 Colburn factor for different fin spacings and Reynolds number

ACKNOWLEDGEMENTS

The work reported here forms a part of the Department of Science and Technology, Government of India, New Delhi sponsored project 'Modelling and Computation of Three-Dimensional Turbulent Convective Heat Transfer for Design of Energy Efficient Pin Fin Heat Exchanger' (SR/S3/MERC-091/2007). A. Dewan and P. Mahanta acknowledge the financial support received from DST.

© Authors 2010

REFERENCES

1 **Kays, W. M.** Pin fin heat exchanger surfaces. *Trans. ASME*, 1955, **77,** 471–483.
2 **Dewan, A., Mahanta, P., Sumithra Raju, K.,** and **Suresh Kumar, P.** Review of passive heat transfer augmentation techniques. *Proc. IMechE, Part A: J. Power and Energy*, 2004, **218**(A7), 509–527. DOI: 10.1243/0957650042456953.
3 **Maudgal, V. K.** and **Sunderland, J. E.** An experimental study of forced convection heat transfer from inline pin fin arrays. In Proceedings of the 13th IEEE Semi-Therm Symposium, Austin, Texas, USA, 1997, pp. 149–157.

4 **Behnia, M., Copeland, D.,** and **Soodphakdee, D.** A comparison of heat sink geometries for laminar forced convection: numerical simulation of periodically developed flow. In Proceedings of the InterSociety Conference on *Thermal phenomena*, Seattle, Washington, USA, 1998, pp. 310–315.

5 **Leon, O., Mey, G. D., Dick, E.,** and **Vierendeels, J.** Comparison between the standard and staggered layout for cooling fins in forced convective cooling. *J. Electron. Pack.*, 2003, **125**, 442–446.

6 **Short, Jr, B. E., Price, D. C.,** and **Raad, P. E.** Design of cast pin fin coldwalls for air-cooled electronics systems. *J. Electron. Pack.*, 2004, **126**, 67–73.

7 **Kobus, C. J.** and **Oshio, T.** Development of a theoretical model for predicting the thermal performance characteristics of a vertical pin-fin array heat sink under combined forced and natural convection with impinging flow. *Int. J. Heat Mass Transf.*, 2005, **48,** 1053–1063.

8 **Tahat, M., Kodah, Z. H., Jarrah, B. A.,** and **Probert, S. D.** Heat transfers from pin-fin arrays experiencing forced convection. *Appl. Energy*, 2000, **67**, 419–442.

9 **Sahiti, N., Durst, F.,** and **Dewan, A.** Strategy for selection of elements for heat transfer enhancement. *Int. J. Heat Mass Transf.,* 2006, **49**, 3392–3400.

10 **Sahiti, N., Durst, F.,** and **Dewan, A.** Heat transfer enhancement by pin elements. *Int. J. Heat Mass Transf.,* 2005, **48**, 4738–4747.

11 **Sparrow, E. M., Ramsey, J. W.,** and **Altemani, C. A. C.** Experiments on inline-pin fin arrays and performance comparison with staggered arrangement. *ASME J. Heat Transf.*, 1980, **102**, 44–50.

12 **Metzger, D. E., Berry, R. A.,** and **Bronson, J. P.** Developing heat transfer in rectangular ducts with staggered arrays of short pin fin. *ASME J. Heat Transf.*, 1982, **104**, 700–706.

13 **Moshfegh, B.** and **Nyiredy, R.** Comparing RANS models for flow and thermal analysis of pin fin heat sinks. In Proceedings of the 15th Australasian Fluid Mechanics Conference, University of Sydney, Sydney, 2004.

14 **Dewan, A., Dayanand, L.,** and **Patro, P.** Mathematical modeling and computation of three-dimensional, turbulent, convective heat transfer in a heat exchanger with circular pin fins. In *Applied mathematical modeling* (Ed. E. N. Virtanen), 2008, pp. 273–296 (Nova Publishers, New York).

15 **Ames, F. E.** and **Dvorak, L. A.** Turbulent transport in pin fin arrays: experimental data and predictions. *J. Turbomach.*, 2006, **128**, 71–81.

16 **Dvinsky, A., Bar-Cohen, A.,** and **Strelets, M.** Thermofluid analysis of staggered and inline pin fin heat sinks. In Proceedings of the Inter Society Conference on *Thermal phenomena*, 2000, pp. 157–164.

17 **Stanescu, G., Fowler, A. J.** and **Bejan, A.** The optimal spacing of cylinders in free-stream cross-flow forced convection. *lnt. J. Heat Mass Transf.*, 1996, **39**, 311–317.

18 **Zukauskas, A.** and **Ulinskas, R.** Efficiency parameters for heat transfer in tube banks. *Heat Transf. Engng*, 1983, **36**, 19–25.

19 **Zukauskas, A.** *Heat transfer from tubes in cross flow, advances in heat transfer*, vol. 8, 1972, pp. 93–160 (Academic Press, New York).

20 **Larson, E. D.** and **Sparrow, E. M.** Performance comparison among geometrically different pin fin arrays situated in an oncoming longitudinal flow. *Int. J. Heat Mass Transf.*, 1982, **25**, 723–725.

21 **Ames, F. E., Dvorak, L. A.,** and **Morrow, M. J.** Turbulent augmentation of internal convection over pins in staggered pin-fin arrays. *J. Turbomach.*, 2005, **127**, 183–190.

22 **Lu, B.** and **Jiang, P. X.** Experimental and numerical investigation of convection heat transfer in a rectangular channel with angled ribs. *Exp. Therm. Fluid Sci.*, 2006, **30**, 513–521.

23 **Incropera, F. P**. *Liquid cooling of electronic devices by single phase convection*, 1999 (John Wiley, New York).

24 **Tahat, M. A., Babus'Haq, R. F.,** and **Probert, S. D.** Forced steady-state convections from pin-fin arrays. *J. Appl. Energy*, 1994, **48**, 335–351.

25 **Mon, M. S.** and **Gross, U.** Numerical study of fin-spacing effects in annular-finned tube heat exchangers. *Int. J. Heat Mass Transf.,* 2004, **47**, 1953–1964.

26 **Yang, K. S., Chiang, C., Lin, Y., Chien, K.,** and **Wang, C.** On the heat transfer characteristics of heat sinks: influence of fin spacing at low Reynolds number region. *Int. J. Heat Mass Transf.*, 2007, **50**, 2667–2674.

27 **Sahin, B.** A Taguchi approach for determination of optimum design parameters for a heat exchanger having circular-cross sectional pin fins. *Int. J. Heat Mass Transf.,* 2007, **43**, 493–502.

28 **Babus'Haq, R. F., Akintunde, K.,** and **Probert, S. D.** Thermal performance of a pin-fin assembly. *Int. J. Heat Fluid Flow*, 1995, **16**, 50–55.

29 **Goldstein, R. J., Ibele, W. E., Patankar, S. V., Simon, T. W., Kuehn, T. H., Strykowski, P. J., Tamma, K. K., Heberlein, J. V. R., Davidson, J. H., Bischof, J., Kulacki, F. A., Kortshagen, U., Garrick, S.,** and **Srinivasan, V.** Heat transfer – a review of 2003 literature. *Int. J. Heat Mass Transf.*, 2006, **49**, 451–534.

30 **Sahiti, N., Lemouedda, A., Stojkovic, D., Durst, F.,** and **Franz, E.** Performance comparison of pin fin in-duct flow arrays with various pin cross-sections. *Appl. Therm. Engng*, 2006, **26**, 1176–1192.

31 **Sahiti, N.** *Thermal and fluid dynamic performance of pin fin heat transfer surfaces*. PhD Thesis, University of Erlangen Nuremberg, Germany, 2006.

32 *FLUENT 6.3 users guide*, 2006 (Fluent Inc., Lebanon, USA).

33 **Kwak, K. M., Torii, K.,** and **Nishino, K.** Simultaneous heat transfer enhancement and pressure loss reduction for finned-tube bundles with the first or two transverse rows of built-in winglets. *Exp. Therm. Fluid Sci.*, 2005, **29**, 625–632.

APPENDIX

Notation

C_p	specific heat at constant pressure
C_f	friction coefficient
d	diameter of fins
D_h	hydraulic diameter
H	fin height
h	heat-transfer coefficient
J	Colburn factor
k	thermal conductivity

k	turbulent kinetic energy
L	length
Nu	Nusselt number
p	pressure
Pr	Prandtl number
Q	heat flux
Re	Reynolds number
S	longitudinal fin spacing
St	Stanton number
T	temperature
U	inlet air velocity
y^+	non-dimensional distance from wall
δ_{ij}	Kronecker delta
Δ	drop
ε	dissipation rate
μ	dynamic viscosity
ρ	density
τ	shear stress

Subscripts

a	air
f	fluid
h	hydraulic
t	turbulent
w	wall